Stereolithography-Based Hydrogel Microenvironments to Examine Cellular Interactions

*Pinar Zorlutuna, Jae Hyun Jeong, Hyunjoon Kong, and Rashid Bashir**

A spatially organized three-dimensional (3D) co-culture of multiple cell types is required to recapitulate cellular interactions and microenvironments in complex tissues. Although there are limited reports for 3D patterning of cells and materials, approaches to examine functional interactions of 3D spatially patterned multiple cell types are lacking entirely. This is mostly due to difficulties in controlling the physical arrangement of cells in a 3D matrix and the physical properties of the cell-encapsulating matrix, while keeping the cells alive and functional for extended periods of time. In this study, an automated maskless fabrication technique is combined with a tunable polymer blend to spatially organize primary hippocampus neurons (HNs) and skeletal muscle myoblast cells (MCs) in a 3D hydrogel matrix with tunable mechanical and degradation properties. The spatial organization of these multiple cell types revealed that the presence of MCs resulted in increased cholinergic functionality of the HNs, as quantified by their choline acetyltransferase activity. The presence of a factor alone is not sufficient, but its spatiotemporal control is necessary; a condition that is possibly true for many cellular interactions. Therefore, the system described here offers a different approach to examine such previously unknown interactions. The approach proposed in this study can be used to examine interactions between many different cell types and shift the 3D fabrication paradigm to a next level, which is to fabricate tissues that are not only viable but also functional.

1. Introduction

Engineering complex three-dimensional (3D) tissues presents great promises to improve treatment of tissue defects and to provide a better understanding of the behavior of normal and pathologic cells. Hence, there is an immediate need for systems that can recapitulate and further manipulate the tissues of interest in a high throughput and automated manner, while maximizing the cell and tissue functionality. Many studies report the development or optimization of techniques for spatially organized and complex 3D tissue fabrication.[1–10] Among these techniques, layer-by-layer photolithography, commonly referred to as stereolithography (SL), is one of the most promising approaches. SL is a maskless computer aided design (CAD)-based rapid prototyping technique that can fabricate complex 3D structures with feature sizes ranging from a few micrometers to centimeters, and with the option of incorporating matrices with varied properties and structure.[1] Current studies clearly demonstrate the capabilities of these fabrication approaches on 3D spatial patterning of bioactive molecules,[2] cells,[3–5] or materials.[6,7] Nevertheless, in these studies limited or no cell culture experiments are reported, often with a demonstration of cell viability only, leaving the functionality of the cells unexplored. It is noteworthy that only in a few of these studies the function of cells that are seeded on[8] or encapsulated inside[10] these hydrogels are examined, while interactions of more than one cell type are not examined. In the majority of these studies, cells were seeded after scaffold fabrication rather than being encapsulated during fabrication,[2,7–9] therefore many advantages of cell-laden hydrogels remain unexploited.[11] These advantages include accommodating cells in a 3D and fully hydrated environment similar to their native one, co-culturing more than one cell type with control over their spatial organization, higher yields of cell densities, and a more uniform cell distribution compared to cell seeding. Furthermore, the lack of cells in the fabrication step is inconsistent with the paradigm of high throughput and automated tissue fabrication. Hence, it can be suggested that a large gap exists between the development of 3D fabrication methods and their ability to regulate cell–cell or cell–environment interactions towards the control of cellular phenotypes. This gap is related to fabrication methods

Dr. P. Zorlutuna, Dr. R. Bashir
Department of Electrical and Computer Engineering
University of Illinois at Urbana-Champaign
Urbana, Illinois 61801, USA
E-mail: rbashir@illinois.edu
Dr. R. Bashir
Department of Bioengineering
University of Illinois at Urbana-Champaign
Urbana, Illinois 61801, USA
Dr. J. H. Jeong, Dr. H. Kong
Department of Chemical and Biomolecular Engineering
University of Illinois at Urbana-Champaign
Urbana, Illinois 61801, USA
Dr. P. Zorlutuna, Dr. H. Kong, Dr. R. Bashir
Micro and Nanotechnology Laboratory
University of Illinois at Urbana-Champaign
Urbana, Illinois 61801, USA
Dr. H. Kong, Dr. R. Bashir
Institute of Genomic Biology
University of Illinois at Urbana-Champaign
Urbana, Illinois 61801, USA

DOI: 10.1002/adfm.201101023

that are not optimized for cell encapsulation, combined with a limited choice of polymers that can be used with these fabrication methods while maintaining cell viability.

This study aims to create a well-defined 3D co-culture environment and to exploit it to investigate and quantify the spatial interaction of two cell types that can interact to regulate their phenotypic activities. In the current study, we used a novel tunable and degradable polymer with a SL system, which resulted in an improvement in cellular viability and cell spreading. Further, we improved the patterning capability of our system, and a layer-by-layer fabrication process in the *x*, *y*, and *z* dimensions is demonstrated. Finally, we show biological functionality and the changes upon interaction with other cells encapsulated in the polymer. MCs and HNs were used to show enhanced neuronal functionality due to factors released by the MCs. We used a hydrogel consisting of oxidized methacrylic alginate (OMA) linked with optional cell adhesion oligopeptides, containing a Arg-Gly-Asp (RGD) sequence and poly(ethylene glycol) methyl ether methacrylate (molecular weight (M_w) 1100 Da, PEGMA1100), for fabricating 3D multicellular constructs with an SL apparatus (SLA). The fabrication process was modified and optimized to accommodate patterning of multiple cell and material types. OMA was previously synthesized to independently control stiffness, permeability, and degradation rate of PEGMA1100 hydrogel, which displays the intricate dependency between properties.[12,13] The hydrogels prepared in this study were characterized for their mechanical properties, degradation rate, and biocompatibility. C2C12 myoblast cells (MC), a PC12 neuron-like cell line, adipose-derived stem cells (ASC) and primary rat hippocampal neurons (HN) were encapsulated together or separately to assess the fabrication capabilities with multiple cell types, to quantitatively investigate cell viability and spreading, and to quantify cell–cell interaction and cell functionality through patterned co-encapsulation. Such systems can be very useful to gain a deeper understanding of how cooperative cell behavior leads to the formation of large organized cellular structures (i.e., neuro–muscular junctions), while their applications can be used to create novel implantable scaffolds in which multiple cell types coordinate to perform a specified function.

2. Results and Discussions

2.1. 3D Hydrogel Fabrication

Alginate molecule was first rendered degradable through oxidation, then made photocrosslinkable by reacting with 2-aminoethylmethacrylate, and finally functionalized by conjugating RGD peptides to the polymer. The resulting OMA was mixed with PEGMA1100 for fabricating hydrogels through photocrosslinking (**Figure 1**A). For crosslinking, an SLA was used, which utilizes a UV laser (325 nm) and a computer controlled elevator (100–250 μm step size) that allows automated fabrication of complex 3D shapes in a layer-by-layer fashion. The initial modulus (E_0) of the fabricated hydrogel was ca. 12 kPa, which is ideal for culturing skeletal muscle tissue (Figure 1B).[14] The initial number of elastically effective crosslinks (N_0), calculated from the elastic modulus (E) and swelling ratio (Q) (see Equation 2 and Figure S2 in the Supporting Information), was independent of the number of oxidized uronic acid (oUA) residues in the alginate molecule (Figure 1B). In contrast, the hydrogel degradation, quantified with a decrease of the number of elastically effective crosslinks (N), normalized with N_0 over time, increased by the increasing the number of oUA residues of OMA (Figure 1C). This results show that the hydrogel degradation rate was controlled by the number of oUA residues of OMA, irrespective of N_0. Figure S1 shows a CAD model of a human head (left) and an image of the hydrogel fabricated using this model in 56 layers (right). With this layer-by-layer mechanism the SLA provides an inherent ability to change the solution type that is added in each layer, if the system is modified and optimized properly.

2.2. Muscle Cell Encapsulation

We first assessed the effect of oxidation on cell viability in gels polymerized in the SLA. MCs were encapsulated in OMA–PEGMA1100 gels with different numbers of oUA residues (3, 6, and 10% oUA). A MA–PEGMA1100 hydrogel was used as a positive control, which was demonstrated to maintain cell viability at a high level. Results of a MTS (3-(4,5-dimethylthiazol-2-yl)-5-(3-carboxymethoxyphenyl)-2-(4-sulfophenyl)-2H-tetrazolium) assay showed that, up to 6% oUA content, the initial cell viability in the gels was the same as in the MA control, while 10% oUA caused a significant drop in viability, possibly due to toxicity caused by the aldehyde groups in oUA (**Figure 2**A). The long-term viability of MCs showed no significant difference between the test groups after the first 24 h, indicating that OMA with 3% and 6% oUA residues are as biocompatible as PEGDA3400, a widely used hydrogel for cell encapsulation (Figure 2B). After an initial decrease on day 4, MCs in the hydrogel consisting of PEGMA1100 and OMA with 6% oUA remained viable until day 14, with no further significant drop in the cell viability, and the cells in it survived significantly more comapred to other test groups. Specifically, the cell viability level was 1.8 times higher than the cells cultured in hydrogels prepared with OMA containing 3% oUA, and 2.5 times higher than the cells cultured in a PEGDA3400 hydrogel. This enhanced viability is probably related to the hydrogel degradation, which provides cells with more space for spreading and increased diffusion of nutrients and waste, caused by an increased swelling ratio.

Further modification of the hydrogel with RGD peptides showed significant cell spreading and fusion. Fluorescence microscopy images of MCs in the hydrogel of PEGMA1100 and OMA with 6% oUA gels, stained for actin filaments and counter stained with DAPI (4′,6-diamidino-2-phenylindole), revealed extensive cell fusion and large tubelike formations within these gels (Figure 2C–F). The tubelike formation is a result of further interaction of closely located, already spread cells. Some cells are spread separately in the rest of the hydrogel, while some other form network structures that ultimately form cell dense tubelike structures, as shown in Figure 2C. The degree of spreading was also quantified using ImageJ[15] to calculate the cell area in the hydrogels over 14 days (Figure 2G). This was further examined

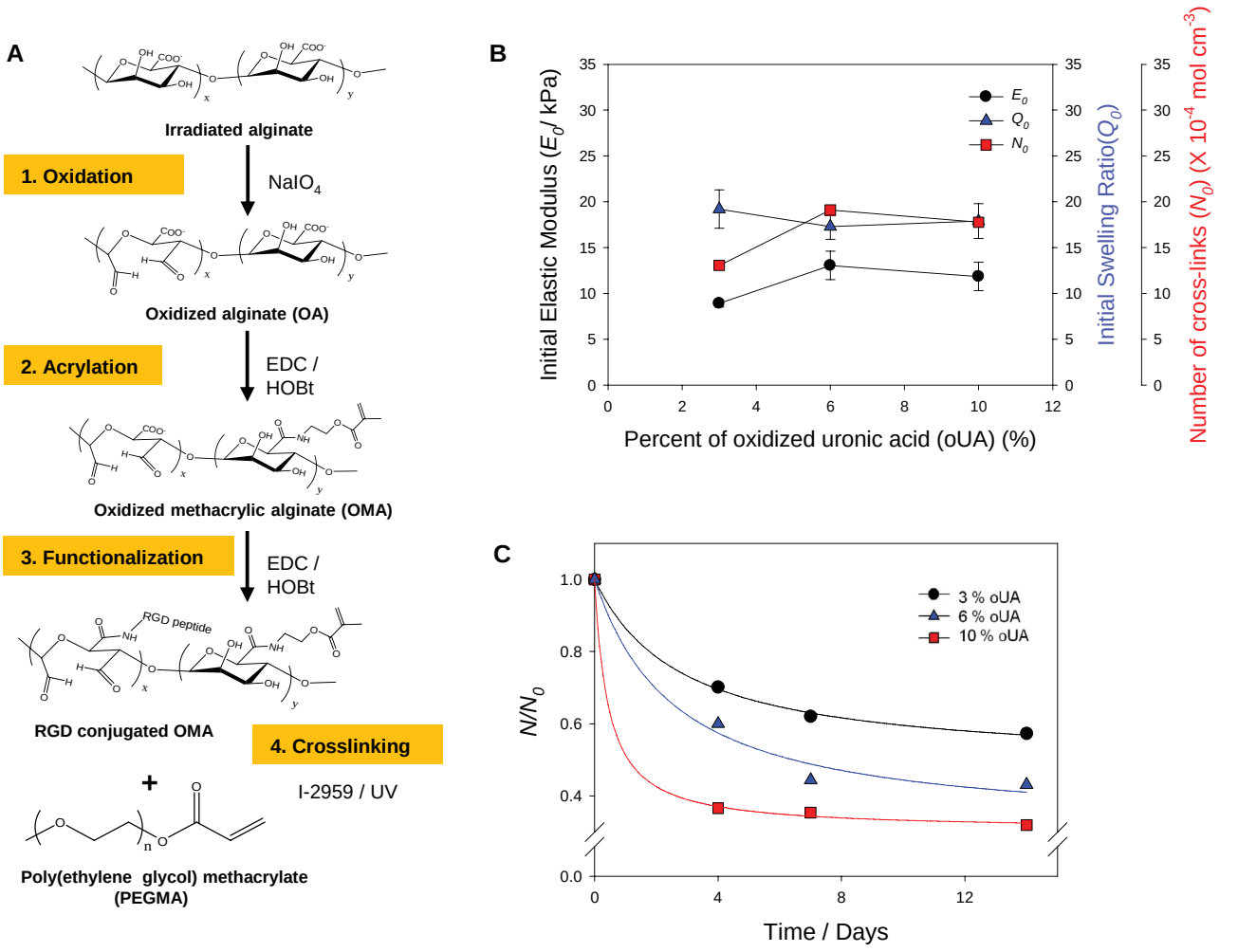

Figure 1. Synthesis of a trifunctional alginate for fabricating a biodegradable and cell-adherent hydrogel using SL. A) Alginate was rendered degradable (step 1), UV crosslinkable (step 2), functionalized with RGD (step 3), and then mixed with PEGMA1100 for in situ cell encapsulation through UV crosslinking. B) The initial number of elastically effective crosslinks (N_0) of OMA–PEGMA1100 hydrogels is independent of the number of oxidized uronic acid (oUA) residues in the OMA. C) An increase in the number of oUA residues of the OMA accelerated the decrease of N with time, which was used to quantify the degradation profile of the hydrogels. N measured at each time point was normalized with N_0 calculated from the initial elastic modulus (E) and the swelling ratio (Q) of the hydrogels.

qualitatively using brightfield microscopy (Figure S3A–C) and two-photon laser scanning microscopy (LSM) (Figure S3D–F in the Supporting Information). As a comparison, 3% oUA was also quantified for cell spreading (Figure S4 in the Supporting Information). In previous studies, we have shown that the swelling behavior, stiffness, toughness, and degradation behavior of MA and OMA can be controlled independently, a very important issue in examining cell–environment interactions.[12,13] Previous studies with alginate showed that, while alginate itself was inert for cell attachment and spreading, the cell adhesion properties of alginate can be tailored by controlling the amount of RGD that is linked to its backbone.[16] Our studies with the same type of cells (i.e., C2C12 myoblast cells), but encapsulated in a 3D fashion instead of seeding on the surface of the gels, and a modified alginate polymer (i.e., OMA) showed a similar result (Figure 2). MCs did not spread at all in the absence of RGD groups linked to OMA–PEGMA1100, while extensive cell spreading was observed with the conjugated RGD. This result suggests that the cell adhesion properties of OMA–PEGMA1100 can be tailored with bioactive groups (i.e., RGD), independent of the oUA amount and the stiffness of the material. Finally, incorporating this material with a complex 3D fabrication method provides a unique method for examining cell–environment interactions.

2.3. Hippocampal Neuron Encapsulation

Since we want to explore the use of primary cells in the SLA system, we also included a neuronlike PC12 cell line to compare their viability with primary HNs. Both cell types were encapsulated in the hydrogel of PEG1100 and OMA with 6% oUA (OMA–PEGA1100, 6% oUA) and assessed for their viability for 14 days. The polymerization was performed in the SLA.

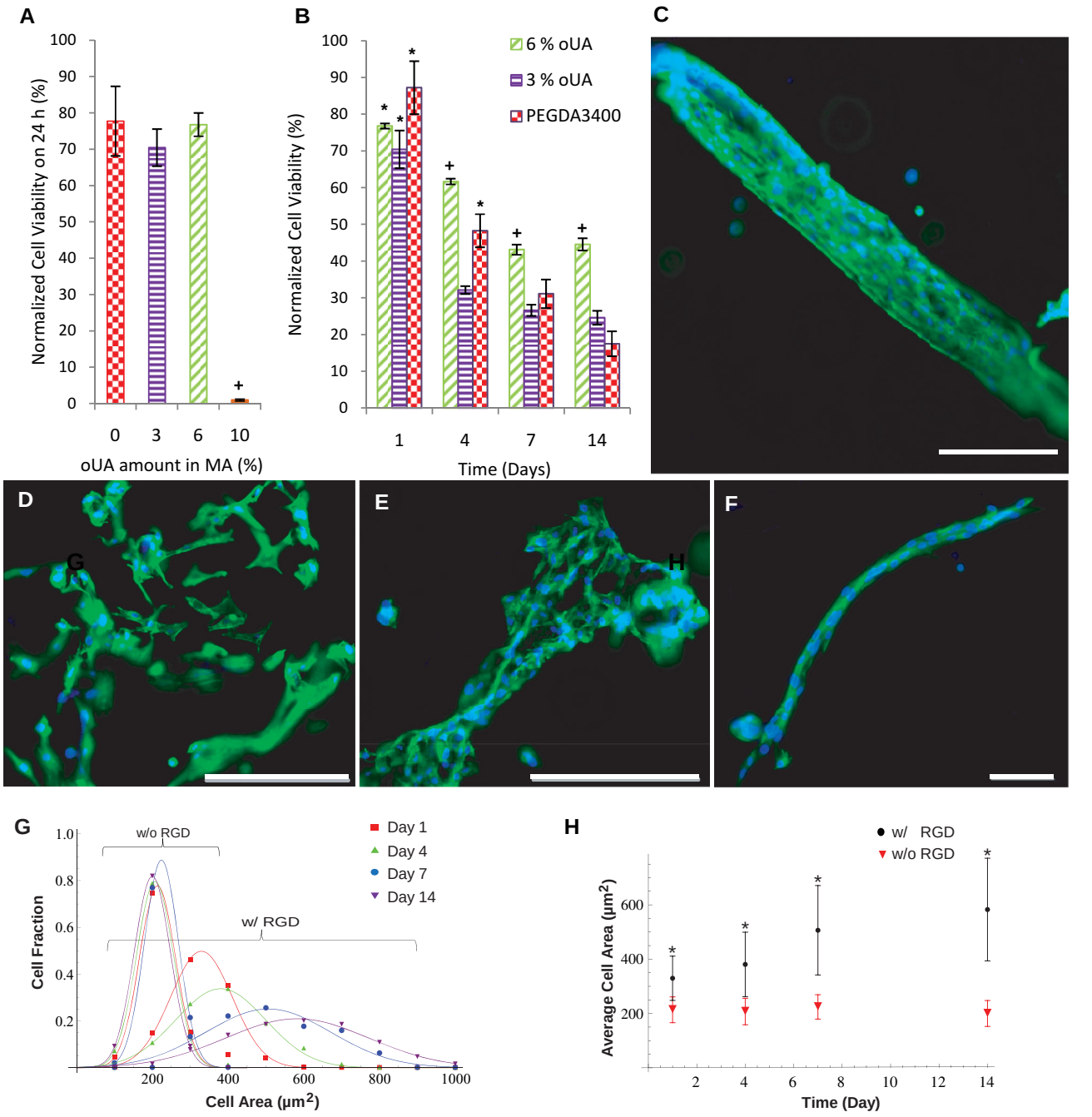

Figure 2. MCs were encapsulated using an SLA and characterized for their viability, spreading, and cell fusion. The viability of MCs in different OMA–PEGMA1100 hydrogels was quantified using MTS (the data are normalized to the day 0 value of each group, $n > 3$, the error bars represent the standard deviation (SD), * indicates the significance within a group ($p < 0.001$), and + indicates the significance among the groups ($p < 0.001$)). A) MC viability after 24 h in OMA–PEGMA1100 with different oxidation degrees, B) MC viability over 14 days in OMA–PEG1100 with 3% oUA, OMA–PEGMA1100 with 6% oUA, and in PEGDA3400 (a control for a nondegrading, biocompatible gel). MCs spreading in OMA–PEGMA1100 (6% oUA) hydrogels. C–F) Fluorescence microscopy images of the MCs in OMA–PEG1100 (6% oUA) hydrogels on day 14, stained with DAPI and Phalloidin-Alexa488 (scale bar = 200 μm in all images). G) The spreading was quantified as the cell area that was measured using ImageJ over 14 days in gels with (w/) and without (w/o) RGD groups. The data are fit to a normal distribution. H) Average cell area throughout the culture duration (error bars represent the standard deviation (sigma) of the fit curves, * indicates the significance within and among the groups ($p < 0.001$), $n \approx 150$ cells from 3 different gels).

According to MTS studies the number of viable cells remained constant, both for the PC12s and for the HNs (**Figure 3**A). At the end of day 14, HNs were examined via immunohistochemistry using MAP2 and counter stained with DAPI. Two-photon LSM showed the neuronal spreading inside the gels, with their processes extending up to hundreds of micrometers (Figure 3B).

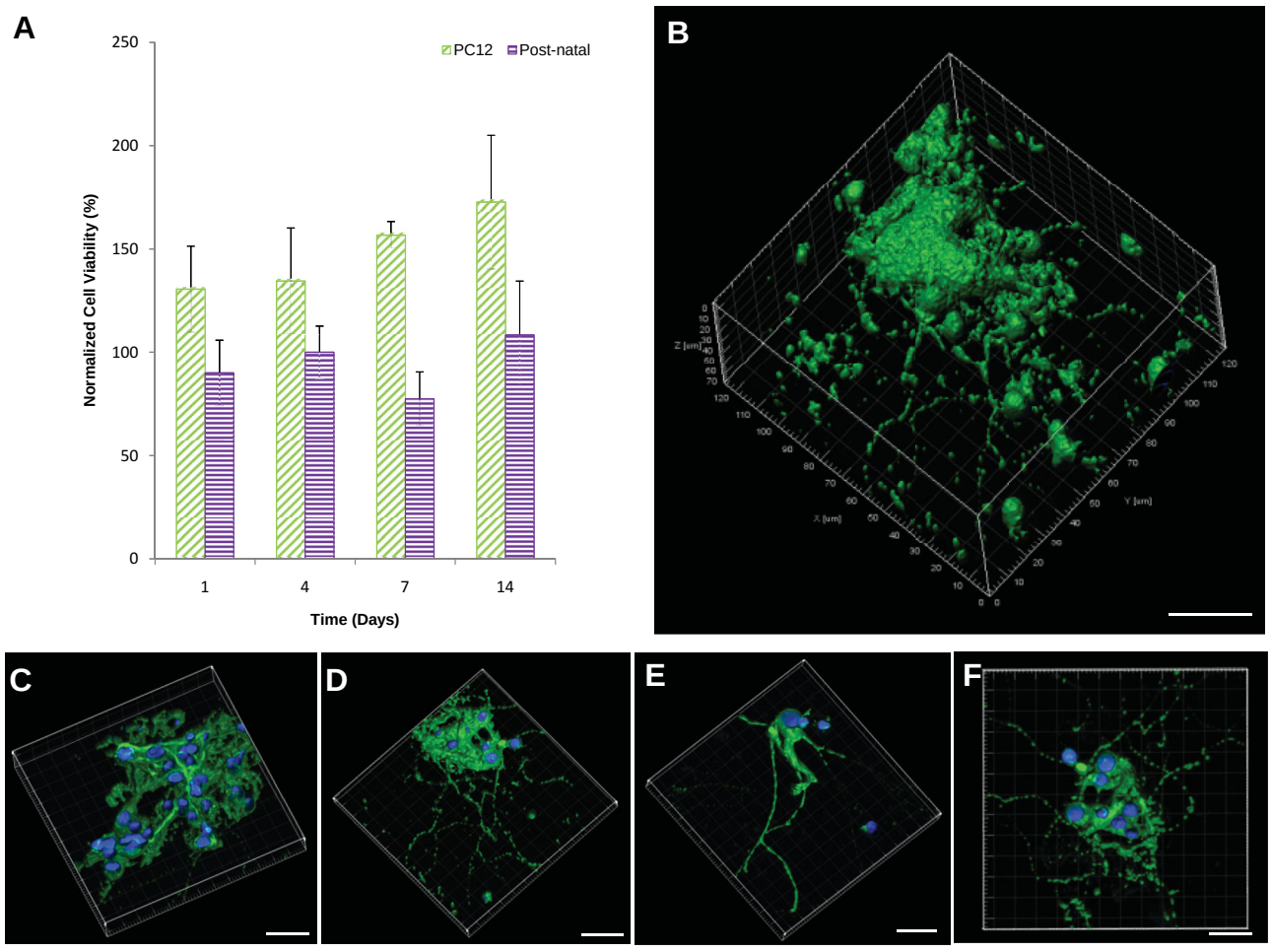

Figure 3. Neurons in OMA–PEGMA1100 (6% oUA) hydrogels. A) HN and PC12 viability quantified using MTS assay for 14 days (data is normalized to the day 0 value of each group, $n = 3$, the error bars represent the SD, there is no significant difference within HNs or PC12s ($p > 0.1$)). Two-photon LSM of HNs was performed on day 14; the cells were stained with DAPI and anti-MAP2 (scale bar is 20 µm). B) A complete *z* stack image showing the cell bodies and the neuronal processes, C–F) Sections from different *z* stacks in order to show the connections between the cells and the cell nuclei.

2.4. 3D Spatial Patterning of Multiple Cell Types

In our previous studies we have shown that it is possible to encapsulate different cell types by using a modified bottom-up approach rather than using the conventional top-down approach of the SLA.[5] After the demonstration of the cell viability of MCs and HNs, described above, we next moved to examine the co-culture of these cell types in three dimensions. In the current study, we added a wash step in between the layers and chose appropriate geometries to demonstrate that it is possible to encapsulate more than one cell and/or material type in the same layer (*xy* patterning) as well as in the subsequent layers (*z* patterning). As a proof of concept, we labeled three different cell types (MCs, HNs, and ASCs) with live cell trackers and constructed 3D patterns with these cells. A square-shaped islands of cell-encapsulating OMA–PEGMA1100 hydrogel was built with regular size and spacing, the the interstitial area was sequentially filled with a hydrogel consisting of poly(ethylene glycol) diacrylates (M_w = 3400 Da, PEGDA3400). **Figure 4**A and B shows the basics of the SL and the steps of the modified fabrication process, respectively. Fluorescence microscopy images show the spatial patterning and compartmentalization of MCs (red) and HNs (green) in OMA-PEGMA1100 and ASCs (blue) in PEG3400 in the same (Figure 4E) or subsequent layers (Figure 4G and H). This spatial organization remained stable during the cell culture period with no significant mixing in between the cell types (Figure 4C and F).

2.5. MC–HN Co-encapsulation and Functional Analysis

Recapitulating multicellular three-dimensional complex tissues is the "holy grail" of tissue engineering and has countless applications in basic science and biomedical fields. The effects of microenvironment stiffness, cell attachment sequences, substrate geometry, and substrate topography on the cell behavior has been one of the main foci of tissue engineering, biomaterials, as well as stem cell research.[17–20] 3D environments that resemble native ones have started to gain more and more attention because of their physiological relevance.[21,22] A particularly

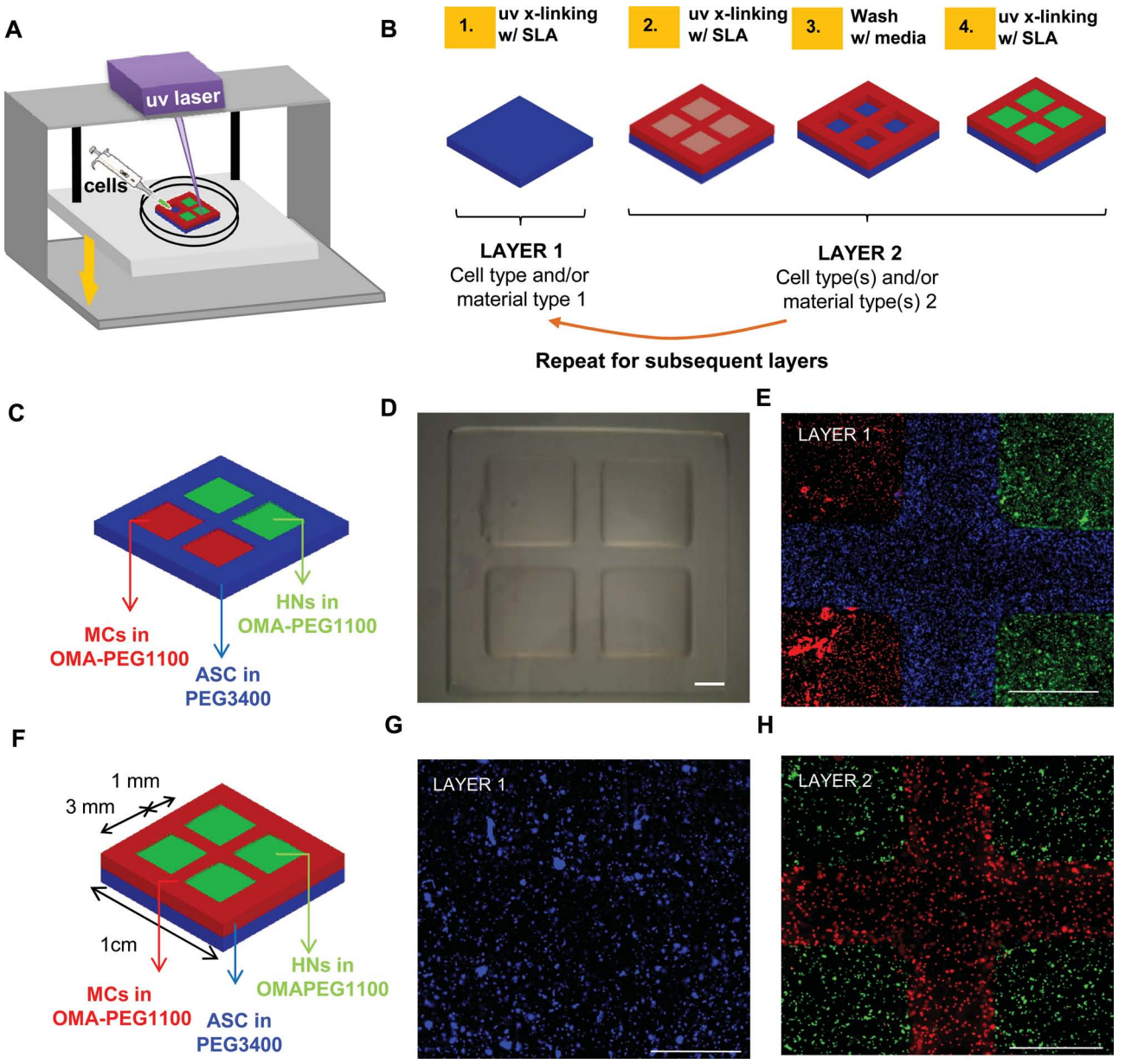

Figure 4. In order to achieve cell patterning in all three dimensions, the SLA was modified and optimized. A) Schematic representation of the SLA. B) Fabrication steps for *xyz* patterning. C) CAD model for fabricating a hydrogel with different cell/material types in the same layer. D) Stereomicroscopy image of the constructed hydrogel. A window frame was fabricated using PEGDA3400, and squares were filled with OMA-PEGMA1100. E) Fluorescence microscopy image of the encapsulated MCs (red), HNs (green), and ASCs (blue), localized at different compartments in the same layer. F) CAD model for fabricating a hydrogel with two different cell types (MCs and HNs) in the same layer, followed by a third cell type (ASCs) encapsulated in the subsequent layer. G) Fluorescence microscopy image of the ASCs (blue) in the first layer, encapsulated in PEGDA3400; H) Fluorescence microscopy image of the MCs (red) and HNs (green) in the second layer, encapsulated in OMA-PEGMA1100 (the scale bar is 1 mm, cells were labeled using CellTracker for live cell tracking, images were taken 24 h after cell encapsulation).

interesting aspect of cell–environment interaction that has not been investigated much is spatially confined cell–cell interaction, where cells nearby can act as a source for bioactive molecules (i.e., paracrine interactions). Recent research on stem cells have also shown that the surrounding cell types play an important role in their differentiation tendencies.[23–25]

We encapsulated MCs and HNs in a spatially organized manner in OMA–PEG1100 (6% oUA) hydrogels through SLA fabrication process. First, MC-encapsulating hydrogels were fabricated in a torus form, and the HN-encapsulating hydrogels were subsequently assembled inside this torus (**Figure 5**A). For control experiments (a HN only culture, and HN only with conditioned media (HN + CM)), the torus was made without adding MCs to the polymer solution. For the MC control, HNs were not included in the polymer solution. Figure 5B shows the MCs encapsulated in the torus (red) and the HNs encapsulated

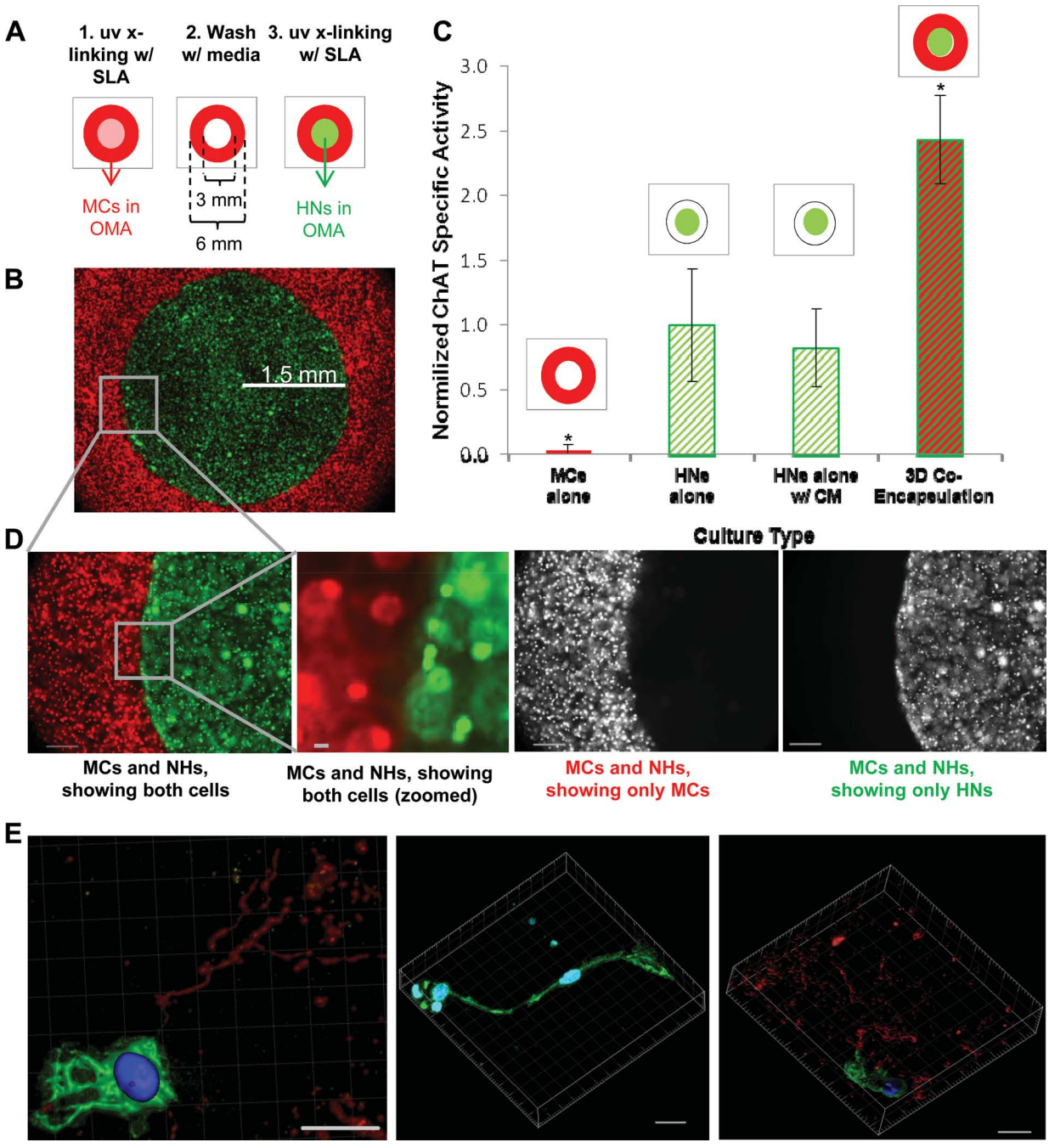

Figure 5. HN functionality in a spatially patterned 3D co-culture with MCs in OMA–PEGMA1100 (6% oUA) hydrogels. A) Schematic outline of the SLA fabrication process. A toroid of MCs in hydrogels was defined with the SLA. Then the unpolymerized portion in the center was washed out, and prepolymer with HNs was placed in the middle and polymerized. B) Florescence image of HN (green) in the middle of the toroid containing MC (red) in the spatially patterned 3D co-culture. C) ChAT specific activity of HNs in different culture conditions after 10 days (CM stands for conditioned medium, $n = 6$, * indicates the significance ($p < 0.001$)). D) Magnified fluorescence images of the 3D spatially patterned co-culture, showing that the cells are not in physical contact but in close proximity (the cells were labeled using CellTracker for live cell tracking, images were taken 24 h after cell encapsulation). E) Two-photon LSM of HNs in the co-culture on day 14, stained with DAPI, anti-tau (red, showing the axons), and anti-MAP2 (green, showing cell body and dendrites) (scale bar is 30 μm).

in the region inside the torus (green), after 24 h of their encapsulation tracked using CellTracker for live cell tracking. The functionality of the neurons inside the hydrogels was quantified through their choline acetyltransferase (ChAT) activity after 10 days of cell culture. The characterized activity was compared to the activity in the presence of MCs, in order to investigate the 3D interaction of these two cell types encapsulated together (Figure 5C). Results show that a ca. 2.5 times increase occured

in the ChAT activity of HNs in a spatially patterned 3D co-culture with MCs, while there was no significant difference in the HNs and HNs + CM control samples. MCs alone did not show any significant ChAT activity, as expected.[26]

The system that we used to co-encapsulate ASCs, MCs, and HNs can be used to examine the differentiation of these stem cells towards neurogenic or myogenic linages, depending on their location with respect to neuronal cells and myoblast cells. Furthermore, the distances between the cells and the material properties can be varied, for example, to assess the dominant factor in the stem cell differentiation (i.e., environment versus surrounding cell type). An alternative approach can be to examine the effect that neurons and myoblasts have on each other, and optionally a stem cell source can be easily incorporated in the culture system, serving as a reservoir for biological factors that might affect this interaction. It is very challenging, if not impossible, to obtain such spatially confined culture models through conventional tissue culture methods and to separate the contact versus noncontact mode of interactions. Therefore, most of the studies examining paracrine effects were either done by co-culturing the cell types together or by using conditioned media. As an example, the difference in contact and paracrine cell–cell interactions was shown using cells seeded on paddles of a movable culture device, and it was found that the hepatocyte functionality can differ depending on their mode of interaction (contact or noncontact) with the nearby fibroblasts.[27]

ChAT synthesizes acetylcholine using choline and acetylCoA as substrates in cholinergic neurons. Although acetylcholine is the major neurotransmitter of the motor neurons that are responsible of actuation of skeletal muscle cells, it is known that some cells in the central nervous system also have this neurotransmitter.[28] The cholinergic neurons in the rat hippocampus, although rare but present in all layers of it, was shown by the immunolabeling of ChAT.[29] The presence of ChAT has long been used for confirming the cholinergic property of a neuron, while its activity has been used as an indicator of its functionality.[29–31] There have been studies examining the effect of muscle-derived factors on cholinergic neurons, mostly on spinal cord neurons, since these cells interact in their natural environment. Co-culturing these cells or using conditioned media from skeletal muscle cells influenced the motor neurons, particularly in a functional manner, by increasing their ChAT activity.[26,32] In addition to skeletal muscle cells, heart muscle cells showed a similar effect, although they are not related to motor neurons directly.[33] Also, this effect is not limited to motor neurons and was shown in other cell types, including neuroblastoma[30] and PC12 cells.[31] The skeletal muscle-related factors causing this effect are collectively referred to as "cholinergic factor".[34] One of the strong candidates for this factor is bFGF (basic fibroblast growth factor); however, there is no consensus, yet, and possibly the effect is caused by a combination of cytokines. Neurons from hippocampus have been shown to possess cholinergic properties.[29] They produce acetylcholine throughout their entire life span, and the amount of it decreases with age.[35] It was also shown that there are stem cells in both adult and embryonic hippocampus that could be used to derive cholinergic neurons.[36] Although not thoroughly examined, some studies investigate the interaction of hippocampal neurons with skeletal muscle cells. It was shown that co-culturing with MCs or using conditioned media from these cells induced some structural changes in hippocampal neurons, namely expression of peripherin, a cytoskeletal protein, which is not expressed in hippocampal neurons in situ.[37] More recently, stem cells isolated from neonatal rat hippocampus was first turned into neurospheres, and then induced to retain cholinergic lineage.[38] The amount of cholinergic neurons in the culture was quantified by the presence of ChAT antigen, and it was significantly more if the neurospheres were cultured in embryonic skeletal muscle cell extract compared to the controls. Nevertheless, to the best of our knowledge, there is no study examining the influence of skeletal muscle on the ChAT activity of hippocampal neurons, and its effect on their functionality as cholinergic neurons. Although it is known that there are cells in the hippocampus producing this enzyme, thus have cholinergic properties,[29] it is interesting that the enzyme's activity is influenced by skeletal muscle-derived factors, since these cells never interact in their natural environment. The cholinergic nature of brain cells is thought to be important for reasons ranging from Alzheimer's disease to aging or stem cell research and development.[35,36,38,39] Therefore, examining such interactions might give insight about the physiology of cholinergic hippocampal cells and might be influential in understanding the cholinergic nature of brain.

In our study, we co-encapsulated HNs with MCs to examine the effect of skeletal muscle-derived factors on the ChAT activity of HNs in a well-defined 3D environment, and then quantified the HN functionality. In order to examine only the paracrine effects and avoid possible influences that might arise from cell-to-cell contact, we exploited our SLA technology to encapsulate these cells in the same hydrogel but in a spatially controlled manner. We also found that conditioning HN media for two days with MCs did not affect the ChAT activity of the HNs significantly, while co-culturing did. One possible explanation is that a sustained and/or time dependent release of the necessary factors is required. Also it might be that the hydrogel is acting as an extracellular matrix for the HN cells, concentrating the paracrine factors released by nearby MCs, while the added conditioned media never reaches adequate concentrations due to diffusion limitations (i.e., factors diffusing from the inside to the outside versus from the outside to the inside). Another possibility is that the effect might depend on the accumulative effects of factors released from the MCs or changes in factors, as the cells mature during the 14 day culture. In the case of conditioned media, on the other hand, MCs were in culture for only the duration of media conditioning, which is two days, ruling out the possibility of sustained or cumulative effects. In any case, our results show an interesting interaction between HNs and MCs, which happens in a spatially patterned 3D co-culture, as compared to conditioned media, implying that there might be more to the simple presence of cholinergic factors, such as spatio-temporal or reciprocal control. It will be essential to conduct more detailed mechanistic studies on the ChAT activity enhanced by co-encapsulation of cells in the future.

3. Conclusions

In conclusion, our culture system, using a multifunctional polymer with SLA to control spatial distribution and adhesion

of multiple cell types, allowed us to examine the reciprocal interaction between two different cell populations in an environment close to their natural 3D environment, demonstrating their interaction and, in turn, functional enhancement. MCs spread extensively throughout the hydrogel during the 14 day culture period and formed tube-like structures, while HNs extended their processes throughout the gel. The spatially patterned 3D co-culture of these two cell types resulted in significantly enhanced functionality of HNs, quantified by their ChAT activity. This result is particularly interesting, because it shows that this interaction is not limited to the native skeletal-muscle-motor–neuron couple, but can be recapitulated with similar cell types (i.e., hippocampal neurons). This finding might be useful for gaining a deeper understanding about the nature of muscle–neuron interaction, while the system itself can be extended to various other cell pairs or triplets. Our findings show that combining this material with the SLA system for precise control of spatial organization of cells (while allowing computer-aided design-based rapid prototyping technology and automated fabrication of complex 3D tissues) can be used for tissue engineering applications or for the fabrication of multicellular biological systems.

4. Experimental Section

Hydrogel Fabrication and Characterization: OMA was synthesized starting from commercially available alginate, rich in gluronic acid residues (LF20/40, FMC Technologies, $M_w \approx 250\,000$ Da) by following a previously published protocol.[13] RGDS- (Sigma–Aldrich) conjugated OMA was prepared by aqueous carbodiimide chemistry of the synthesized OMA and RGD (1.6%) at room temperature for 12 h. The polymer solution consisted of 3% OMA (with different oUA residues), 20% PEGMA1100, and 0.5% I2959 (1-(4-(2-hydroxyethoxy)-phenyl)-2-hydroxy-2-methyl-1-propane-1-one (Irgacure 2959, Ciba, Tarrytown, NY), prepared in DMSO) in DMEM. As a control for cell viability studies and for multi-material fabrications poly(ethylene glycol) diacrylate $M_W = 3400$ Da (PEGDA3400, Laysan Bio, Arab, AL) was used. The composition of PEGDA3400 polymer solution was 20% PEGDA3400, 0.5% I2959 (in DMSO, vortexed for dissolving), 5 mM RGDS (conjugated to acrylate-PEG3500-NHS (JenKem Technology, Allen, TX)) in DMEM. Hydrogels were fabricated using a stereolithography apparatus (SLA, Model 250/50, 3D Systems, Rock Hill, SC, USA) in all experiments. The SLA was modified and optimized as described previously and used for patterning multiple cell and material types in predetermined regions of the construct.[5] If fabrication was done with more than one material and/or cell types in a layer, a wash step was added to the process, and the elevator was kept at the same position as the previous layer until a new layer was built. Different material/cell types can be incorporated to subsequent layers without the wash step. The process was repeated until completion of the desired complex 3D structure. Hydrogels were characterized for their mechanical properties as described previously.[5] For degradation studies, measurements were repeated for 14 days.

Cell Encapsulation: Primary hippocampal neurons (HNs) were isolated form Sprague–Dawley rats (1 to 3 days postnatal), in accordance with PHS guidelines for the humane treatment of animals under approved protocols established through the University of Illinois at Urbana-Champaign Institutional Animal Care and Use Committee under the Vice Chancellor for Research, following a well-established protocol and used immediately for encapsulation.[40] ASCs (gift from Prof. Lawrence B. Schook, Dept. of Animal Science, UIUC, IL) and C2C12 myoblasts (MCs, ATCC, VA) were incubated in serum-free media (2% HS) after encapsulation. PC12 cells (ATCC, VA) were cultured in F-12K, supplemented with 15% HS and 5% FBS. Prior to encapsulation in hydrogels, the cells were added to the polymer solution and mixed gently (10 000 cells mm^{-3}).

Characterization of Encapsulated Cells: The cell viability in OMA-PEGMA1100 was quantified using the MTS ((3-(4,5-dimethylthiazol-2-yl)-5-(3-carboxymethoxyphenyl)-2-(4-sulfophenyl)-2H-tetrazolium)) assay for 14 days, as described previously.[5] MC spreading inside the hydrogels was examined qualitatively with fluorescence and two-photon LSM and quantitatively using bright-field images and ImageJ,[15] which was used to measure the increase in cell area troughout the culture durations. Immunostaining was performed as described elsewhere.[41] Neuron functionality is assessed by means of ChAT activity using a modified version of the methods in the literature (see the Supporting Information for details).[42]

Statistical Analysis: Statistical significance was determined using one-way ANOVA (analysis of variance) followed by Tukey's Multiple Comparison Test (n and p values of each test are given in the figure legends). All data are presented as mean values, and the error bars represent the standard deviation.

Supporting Information

Supporting Information is available from the Wiley Online Library or from the author.

Acknowledgements

This work was supported by the US Army Telemedicine & Advanced Technology Research Center (TATRC) (W81XWH-08-1-0701) (R.B. and H.J.K.), the National Science Foundation (CAREER: DMR-0847253) (H.J.K.), the American Heart Association (Scientist Development Grant 0830468Z) (H.J.K.), and the National Science Foundation (Science and Technology Center Emergent Behaviors of Integrated Cellular Systems, Grant CBET-0939511) (R.B. and H.J.K).

Received: May 8, 2011
Revised: June 28, 2011
Published online:

[1] F. P. Melchels, J. Feijen, D. W. Grijpma, *Biomaterials* **2010**, *31*, 6121.
[2] L. H. Han, S. Suri, C. E. Schmidt, S. Chen, *Biomed. Microdevices* **2010**, *12*, 721.
[3] H. Tsutsui, E. Yu, S. Marquina, B. Valamehr, I. Wong, H. Wu, C. M. Ho, *Ann. Biomed. Eng.* **2010**, *38*, 3777.
[4] A. Ovsianikov, M. Gruene, M. Pflaum, L. Koch, F. Maiorana, M. Wilhelmi, A. Haverich, B. Chichkov, *Biofabrication* **2010**, *2*, 014104.
[5] V. Chan, P. Zorlutuna, J. H. Jeong, H. Kong, R. Bashir, *Lab. Chip* **2010**, *10*, 2062.
[6] J. W. Choi, E. MacDonald, R. Wicker, *Int. J. Adv. Manuf. Technol.* **2010**, *49*, 543.
[7] K. Arcaute, B. Mann, R. Wicker, *Acta. Biomater.* **2010**, *6*, 1047.
[8] T. M. Hsieh, C. W. Ng, K. Narayanan, A. C. Wan, J. Y. Ying, *Biomaterials* **2010**, *31*, 7648.
[9] F. P. Melchels, K. Bertoldi, R. Gabbrielli, A. H. Velders, J. Feijen, D. W. Grijpma, *Biomaterials* **2010**, *31*, 6909.
[10] V. Liu Tsang, A. A. Chen, L. M. Cho, K. D. Jadin, R. L. Sah, S. DeLong, J. L. West, S. N. Bhatia, *FASEB J.* **2007**, *21*, 790.
[11] G. D. Nicodemus, S. J. Bryant, *Tissue. Eng. Part. B. Rev.* **2008**, *14*, 149.
[12] C. Cha, S. Y. Kim, L. Cao, H. Kong, *Biomaterials* **2010**, *31*, 4864.
[13] C. Cha, R. E. Kohmon, H. Kong, *Adv. Funct. Mater.* **2009**, *19*, 3056.
[14] A. J. Engler, M. A. Griffin, S. Sen, C. G. Bönnemann, H. L. Sweeney, D. E. Discher, *J. Cell. Biol.* **2004**, *166*, 877.

[15] ImageJ, http://rsbweb.nih.gov/ij/(accessed, August 2011).
[16] J. A. Rowley, G. Madlambayan, D. J. Mooney, *Biomaterials* **1999**, *20*, 45.
[17] H. Shin, *Biomaterials* **2007**, *28*, 126.
[18] F. Rehfeldt, A. J. Engler, A. Eckhardt, F. Ahmed, D. E. Discher, *Adv. Drug. Deliv. Rev.* **2007**, *59*, 1329.
[19] H. Park, C. Cannizzaro, G. Vunjak-Novakovic, R. Langer, C. A. Vacanti, O. C. Farokhzad, *Tissue. Eng.* **2007**, *13*, 1867.
[20] A. J. Engler, H. L. Sweeney, D. E. Discher, J. E. Schwarzbauer, *J. Musculoskelet. Neuronal. Interact.* **2007**, *7*, 335.
[21] W. R. Legant, J. S. Miller, B. L. Blakely, D. M. Cohen, G. M. Genin, C. S. Chen, *Nat. Method.* **2010**, *7*, 969.
[22] W. R. Legant, A. Pathak, M. T. Yang, V. S. Deshpande, R. M. McMeeking, C. S. Chen, *Proc. Natl. Acad. Sci. USA* **2009**, *106*, 10097.
[23] J. S. Park, H. N. Yang, D. G. Woo, H. Kim, K. Na, K. H. Park, *Biomaterials* **2010**, *31*, 7275.
[24] S. Trkov, G. Eng, R. Di Liddo, P. P. Parnigotto, G. Vunjak-Novakovic, *J. Tissue. Eng. Regen. Med.* **2010**, *4*, 205.
[25] H. J. Lee, C. Yu, T. Chansakul, S. Varghese, N. S. Hwang, J. H. Elisseeff, *Stem Cells Dev.* **2008**, *17*, 555.
[26] E. L. Giller, J. H. Neale, Jr., P. N. Bullock, B. K. Schrier, P. G. Nelson, *J. Cell. Biol.* **1977**, *74*, 16.
[27] E. E. Hui, S. N. Bhatia, *Proc. Natl. Acad. Sci. USA* **2007**, *104*, 5722.
[28] A. G. Karczmar, *Prog. Brain. Res.* **1990**, *84*, 437.
[29] M. Frotscher, M. Schlander, C. Léránth, *Cell Tissue Res.* **1986**, *246*, 293.
[30] J. L. McManaman, F. G. Crawford, *J. Neurochem.* **1991**, *57*, 258.
[31] D. Schubert, S. Heinemann, Y. Kidokoro, *Proc. Natl. Acad. Sci. USA* **1977**, *74*, 2579.
[32] N. Brookes, D. R. Burt, A. M. Goldberg, G. G. Bierkamper, *Brain Res.* **1980**, *186*, 474.
[33] M. D. Coughlin, E. M. Bloom, I. B. Black, *Dev. Biol.* **1981**, *82*, 56.
[34] D. K. Berg, *Ann. Rev. Neurosci.* **1984**, *7*, 149.
[35] M. Hiramatsu, K. Haba, R. Edamatsu, H. Hamada, A. Mori, *Neurochem. Res.* **1984**, *14*, 249.
[36] E. A. Markakis, T. D. Palmer, M. Randolph-Moore, P. Rakic, F. H. Gage, *J. Neurosci.* **2004**, *24*, 2886.
[37] K. Djabali, A. Zissopoulou, M. J. de Hoop, S. D. Georgatos, C. G. Dotti, *J. Cell. Biol.* **1993**, *123*, 1197.
[38] T. T. Wang, A. H. Jing, X. Y. Luo, M. Li, Y. Kang, X. L. Zou, H. Chen, J. Dong, S. Liu, *NeuroReport* **2006**, *17*, 1433.
[39] J. T. Coyle, D. L. Price, M. R. DeLong, *Science* **1983**, *219*, 1184.
[40] G. J. Brewer, *J. Neurosci. Methods.* **1997**, *71*, 143.
[41] L. J. Millet, M. E. Stewart, J. W. Sweedler, R. G. Nuzzo, M. U. Gillette, *Lab. Chip* **2007**, *7*, 987.
[42] E. J. Menzel, L. R. Walzer, G. Meissl, H. Millesi, *Anal. Chim. Acta* **1988**, *205*, 183.